IOP Publishing Journal of Physics D: Applied Physics
J. Phys. D: Appl. Phys. **51** (2018) 385301 (7pp) https://doi.org/10.1088/1361-6463/aad86f

Realizing fully spin polarized transport in graphene nanoribbons with design of van der Waals vertical heterostructure leads

Xixi Tao[1,2], Peng Jiang[1,2], Lili Kang[1,2], Hua Hao[1,2], Lingling Song[3], Jie Lan[4], Xiaohong Zheng[1,2,5], Lei Zhang[5,6] and Zhi Zeng[1,2]

[1] Key Laboratory of Materials Physics, Institute of Solid State Physics, Chinese Academy of Sciences, Hefei 230031, People's Republic of China
[2] University of Science and Technology of China, Hefei 230026, People's Republic of China
[3] School of Electronic Science and Applied Physics, Hefei University of Technology, Hefei 230009, People's Republic of China
[4] School of Physics and Electronic Engineering, Jiangsu Normal University, Xuzhou 221116, People's Republic of China
[5] State Key Laboratory of Quantum Optics and Quantum Optics Devices, Institute of Laser Spectroscopy, Shanxi University, Taiyuan 030006, People's Republic of China
[6] Collaborative Innovation Center of Extreme Optics, Shanxi University, Taiyuan 030006, People's Republic of China

E-mail: xhzheng@theory.issp.ac.cn and zhanglei@sxu.edu.cn

Received 24 May 2018, revised 18 July 2018
Accepted for publication 7 August 2018
Published 20 August 2018

Abstract

Zigzag-edged graphene and *h*-BN nanoribbons with passivated edges in the ground state are either spin-degenerate or spin-unpolarized systems, which are not directly applicable for spin-polarized transport. In this work, based on density functional calculations, we demonstrate that the combination of them to form van der Waals (vdW) heterostructures can be adopted to realize fully spin polarized transport. As an example, the ballistic transport properties of a zigzag-edged graphene nanoribbon (ZGNR) with six zigzag carbon chains is studied first with each lead as a vdW heterostructure formed by attaching a *h*-BN monolayer to each side of the ZGNR with AA-stacking. A greatly decreased transmission gap (0.28 eV) in one spin and a greatly increased transmission gap (0.82 eV) in the other spin is achieved in the transmission function, resulting in fully spin polarized transport at low bias. This arises from the stagger potential imposed by the *h*-BN layers, which not only exists in the leads, but also extends to the channel region. It changes the energy of the edge states of different spins localized at different sublattices in an opposite way in the whole device. The transmission gap and the threshold voltage can be further modulated by applying a vertical pressure to the vdW leads to tune the strength of the stagger potential or simply by changing the ribbon width. Finally, the increase of the channel length will greatly reduce the magnitude of the transmission around the Fermi level and the transmission gap will eventually recover the value of the band gap of the pristine ZGNR. These findings not only provide a novel way for achieving fully spin polarized transport in graphene, but also demonstrate the great importance of vdW heterostructures in the design of spintronic devices.

Keywords: fully spin polarized transport, stagger potential, van der Waals vertical heterostructure, zigzag graphene nanoribbon

(Some figures may appear in colour only in the online journal)

1. Introduction

Fully spin polarized transport or half-metallic transport has been a long seeking object of numerous studies for many years due to its extreme importance in spintronics since the discovery of half-metallicity originally in Heusler compound [1] and later in many other materials, such as metal-DNA complexes [2], manganese perovskites [3], and organometallic benzene-vanadium wire [4], etc. Starting from the rise of graphene, the ongoing interests and investigations have also led to the prediction of fully spin polarized transport (or half-metallicity) in zigzag-edged graphene nanoribbons (ZGNRs) by a lot of schemes, such as electrical field [5], edge decoration [6], B–N co-doping [7–9], etc. The B–N co-doping scheme is particularly intuitive since the B and N atoms have one less or more electron than carbon and they can affect the carbon systems differently. The combined tuning effects of these two elements have been utilized to achieve many novel functions in carbon systems. Besides the examples of achieving half-metallic transport in graphene nanoribbons with B–N co-doping listed above, another elegant example is the electrical switching effects in metallic carbon nanotubes proposed by Louie *et al* [10], who doped the carbon nanotubes with a B atom and a N atom at the opposite sides of a diameter of the tube. Obviously, new cooperative tuning effects of carbon systems with the B and N atoms are still greatly expectable. However, although all these previously predicted schemes are quite interesting, an absolutely necessary step is that the B and N atoms should be embedded in the graphene lattice, which is generally very difficult, especially since it needs atomic precision control. A natural question that arises is that, can we find a way of using the cooperative tuning effects of B and N atoms without embedding them in the graphene?

It is well known that, in recent years, a new research direction on 2D materials is emerging, which focuses on vertical van der Waals (vdW) heterostructures constructed by stacking different 2D crystals on top of one another [11–18]. In vdW heterostructures, not only the exceptional properties of each layer are well preserved due to the weak vdW interaction that binds the stack layers together, but also new properties or functions may arise. Motivated by the idea of vdW heterostructure and the negligibly small lattice mismatch between hexagonal BN (*h*-BN) sheet and graphene, we may use laterally attached BN nanoribbons to tune the transport properties of ZGNRs. Generally, a device is composed by leads and channel region. In real application, the vdW structure can act either as the channel or as the leads [19–23], and the role as channel or leads will be quite different. As an example, in this work, we will specifically use the graphene-based vdW heterostructures as leads, with which we will demonstrate a different scheme for achieving half-metallic transport in graphene nanoribbons.

In detail, we build a transport junction with an infinite zigzag graphene nanoribbon (ZGNR) which is computationally divided into three regions: left lead, right lead and the central region. Two zigzag-edged *h*-BN nanoribbons (ZBNNRs) with the same ribbon width are attached to the two sides of each lead with AA stacking, but not to the central region which serves as the channel part. Generally, the dangling bonds at the edges of ZGNRs and ZBNNRs will contribute to approximately 1.0 μ_B edge magnetic moment and thus both ZGNRs and ZBNNRs without edge passivation are magnetic [24–26]. However, the edges with dangling bonds are generally not stable and tend to be reconstructed [27], thus they are usually passivated by hydrogen. Hydrogen passivated ZBNNRs are non-magnetic. In this study, we only consider the hydrogen passivated ZGNRs and ZBNNRs. It is found that, although both the individual passivated ZGNRs and ZBNNRs in the ground state are spin-degenerate or spin-unpolarized insulators, the two BN sheets produce a strong stagger potential at their middle plane, which acts differently on the two sublattices of the ZGNR so that the energies of the edge states with different spins shift oppositely. This leads to the lift of the spin degeneracy in the pristine ZGNR, resulting in two greatly different energy gaps $E_{g\uparrow}$ and $E_{g\downarrow}$ for the two spins. As a consequence, fully spin polarized current is obtained at low bias. The transmission gap and the threshold bias can be further modulated by adding a vertical pressure to the vdW leads to tune the strength of the stagger potential. For example, decreasing the interlayer distance by 10% by pressure leads to the closure of the transmission gap and the decrease of threshold bias to nearly zero.

The rest of this paper is organized as follows: in section 2, we present our proposed system, computational details and the theoretical formalism. The numerical results of spin-polarized current are discussed in section 3. Finally, the paper is summarized in section 4.

2. Theoretical formalism and computational details

The ZGNR transport junction with vdW vertical heterostructure leads is presented in figure 1(a). In the leads, the ZGNR is sandwiched between two ZBNNRs, while the channel is composed only by a ZGNR. The transport direction is along the z axis and the width of each ribbon in the x direction contains 6 zigzag chains. Each C/B/N atom at the edge is passivated by a H atom. Due to the same hexagonal lattice structure and the very small mismatching of bond lengths of BN sheet (1.46 Å) and graphene (1.42 Å), the lattice constants of BN ribbons are assumed to be the same as the ZGNR. The layers are stacked together by AA stacking which is more favorable in energy than AB stacking [28]. The distances between two adjacent layers are relaxed to be 3.22 Å. First, to study the general properties and the pressure effect, a channel length with 4 unit cells is considered. Then, to study the length effects of the channel part, three different lengths with 8, 12 and 16 unit cells are considered. For all these junctions, although there are three possible magnetic configurations, namely, anti-ferromagnetic(AFM), ferromagnetic(FM) and nonmagnetic(NM), between the two edges for the ZGNRs, only the ground state (AFM) is considered.

All calculations for electronic structure and ballistic transport are performed by the Nanodcal package [29], which is based on density functional theory (DFT) combined with the non-equilibrium Green's function (NEGF) method [30]. Norm-conserving pseudopotentials and linear combinations

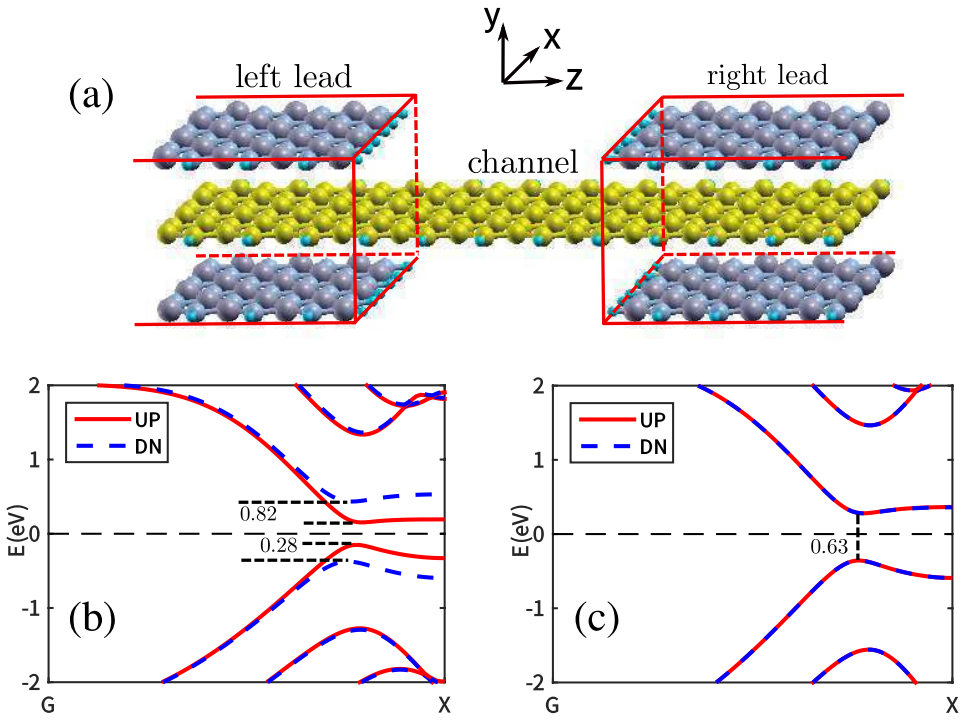

Figure 1. (a) Schematic plot of the ZGNR transport junction with vdW vertical heterostructure leads. It is divided into left lead, right lead and a channel region. In the leads, the ZGNR is sandwiched between two zigzag-edged h-BN nanoribbons. (b), (c) The band structure of the *h*-BN/Gr/ *h*-BN vdW vertical heterostructure and the pristine ZGNR. The numbers indicate the energy gap values.

of the atomic orbitals as basis sets are adopted, and the electron wave functions are expanded with a double zeta polarized (DZP) basis set [31]. The generalized gradient approximation (GGA) with form of Predew–Burke–Ernzerhof (PBE) [32] is applied for the exchange-correlation potential. The vacuum layer between two sheets is chosen as 14.0 Å to avoid inter-layer interaction. The mesh energy cutoff is 200 Ry and the first Brillouin zone of the electrodes is sampled by a $1 \times 1 \times 100$ grid. All structures are fully relaxed until the force convergence criterion of 0.04 eV Å^{-1} is reached.

The spin-dependent transmission $\tau_\sigma(\sigma = \uparrow, \downarrow)$ as a function of energy ε and bias V is calculated by

$$T_\sigma(\varepsilon, V) = Tr[(\Gamma_L(\varepsilon, V)G^r(\varepsilon, V)\Gamma_R(\varepsilon, V)G^a(\varepsilon, V))_{\sigma\sigma}] \quad (1)$$

where $\Gamma_\alpha(\alpha = L, R)$ is the linewidth function which describes the coupling between the α lead and the central region and $G^r(G^a)$ is the retarded (advanced) Green's function. The current through the whole junction at bias V is obtained by integrating the transmission function through the formula

$$I_\sigma(V) = \frac{2e}{h}\int_{\mu_L}^{\mu_R} T_\sigma(E, V)(f(E-\mu_L) - f(E-\mu_R))dE, \quad (2)$$

where h is the Plank's constant, e is the electron charge, $\mu_{L/R} = E_F \pm \frac{eV}{2}$ are the chemical potentials at bias V and $f(E-\mu_{L/R})$ are the Fermi–Dirac distribution functions of electrons in the two electrodes under non-equilibrium conditions.

3. Results and discussion

Firstly, the calculated spin-dependent *I*–*V* characteristics for the whole transport junction with 4 unit cells in the channel region is shown in figure 2(a), in which the most striking feature is the fully spin polarized current at low bias ($V_b \leqslant 0.8$ V). The spin up channel starts from ∼0.3 V while the spin down channel starts from ∼0.8 V. Thus, for $0.3 \leqslant V_b \leqslant 0.8$ V, fully spin polarized transport is achieved. This is in clear contrast to the pristine ZGNR where not only the current is spin unpolarized, but the threshold voltages for both spins are the same (∼0.6 V, not shown). In addition, an obvious negative differential resistance (NDR) starting from 0.7 V is observed, which arises from the relative shift of the band edges of the valence band and conduction band of the two leads under finite bias. The origin of the full spin polarization and threshold voltage can be revealed by analyzing the equilibrium transmission function, which is shown in figure 2(b). It is seen that the transmission gaps for spin down and spin up channel are quite different (0.82 eV for spin down and 0.28 eV for the spin up).

Obviously, the *h*-BN/Gr/ *h*-BN vdW vertical heterostructure leads are responsible for the fully spin polarized transmission in the energy range of 0.82 eV around the Fermi level. To reveal the origin, we calculate the band structure of the *h*-BN/Gr/ *h*-BN vdW vertical heterostructure (see figure 1(b)). In the ground state, the two edges of the single ZGNR are anti-ferromagnetically (AFM) coupled. The maximum magnetic moment of carbon atoms in the two edges is 0.29 μ_B and -0.29 μ_B.

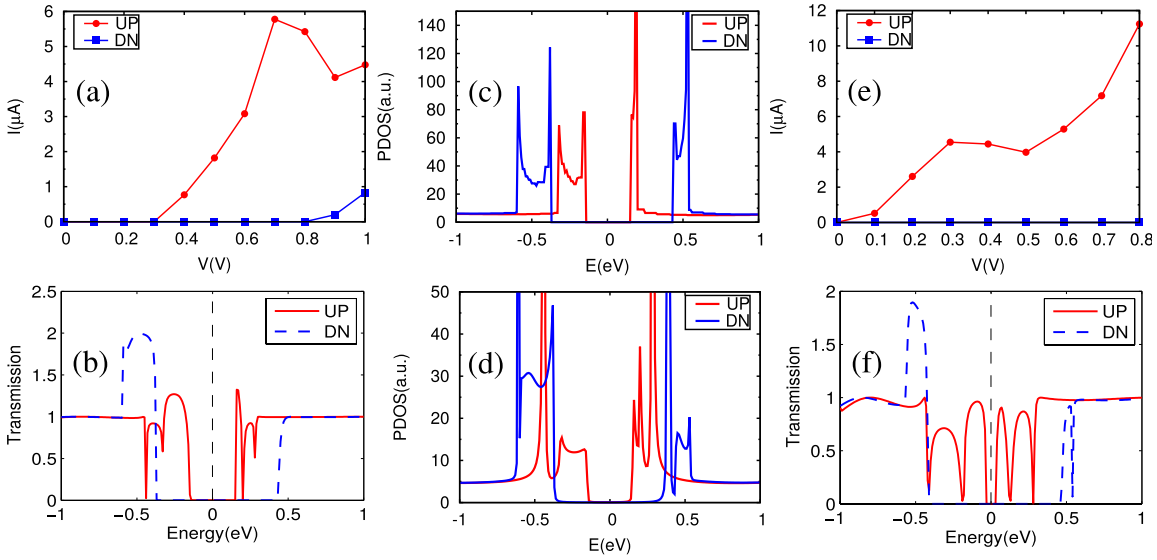

Figure 2. For the transport junction without pressure: (a) the calculated spin-dependent *I*–*V* curve; (b) the calculated equilibrium transmission function; (c), (d) the projected density of states of the lead and of the central unit of the channel region, respectively. For the transport junction with pressure (the two adjacent layers distances are 2.92 Å): (e) the calculated spin-dependent *I*–*V* curve; (f) the calculated equilibrium transmission function. The channel region (the graphene area not covered by BN sheets) contains 4 unit cells.

Note that the band structure of the pristine ZGNR is spin degenerate with a band gap of 0.63 eV (see figure 1(c)). In contrast, as shown in figure 1(b), the spin degeneracy is broken in *h*-BN/Gr/ *h*-BN vdW heterostructure. The band gap for spin up electrons is decreased to $E_{g\uparrow} = 0.28$ eV while that for spin down electrons is increased to $E_{g\downarrow} = 0.82$ eV.

Note that the band gaps of the leads and the transmission gaps are both 0.28 and 0.82 eV for the two spin components, respectively, which are different from the band gap (0.63 eV) of the pristine ZGNR (the channel part in our device). Thus, although the channel part is not sandwiched between two BN sheets, the band gap of this part should have also been changed and smaller than that of the pristine ZGNR since the transmission at any energy must be mediated by some states in the channel. This can be analyzed by the partial density of states (PDOS) of the channel region. Specifically, we show the PDOS of the lead and of the central unit of the channel region for comparison, which are shown in figures 2(c) and (d), respectively. It is seen that although the magnitudes are different, the gaps of the two spin up channels are exactly the same, which explains the the same gap of the transmission function and the band structure of the leads.

Since the full spin polarization is induced by the stagger potential of the BN sheets, the strength of the interaction between the BN sheets and graphene can be decreased or increased by tuning the interlayer distance [28]. Thus, next, we will see what will happen if we decrease the layer distance by 0.30 Å (+9.3%) by pressure. At this pressure, the band gap of the vdW lead decreases to 0.06 eV for the spin up channel. Figure 2(e) shows the *I*–*V* characteristic of the transport junction under pressure. There is only one spin conducting at bias varying from 0.06 to 0.8 V, which exhibits a fully spin polarized *I*–*V* curve. Moreover, the magnitude of the spin polarized current of the junction under pressure is much larger than that under no pressure (see figure 2(a)). The transmission function at equilibrium is also shown in figure 2(f), from which a much decreased transmission gap of 0.06 eV in the spin up channel is observed, exactly the same as the band gap of the vdW lead.

We further investigate the effects of the channel length (see figure 3). The distances between two adjacent layers are fixed as 2.92 Å. The calculated transmission functions for the transport junctions with different channel length $n = 8, 12$ and 16 unit cells are shown in figures 3(a)–(c), respectively. The results show that the transmission gaps of the spin up channel are all 0.06 eV, which suggests that the transmission gaps of the spin up channel are independent of the channel length. However, increasing the channel length greatly affects the magnitude of transmission, which is indicated by a gradual suppression of transmission in the energy range $[-0.3, 0.3]$ eV.

To understand this, it is important to note the fact that, in a device, the transmission is strongly related to the PDOS of the central region, which can be tracked by comparing the changes of the transmission function and the PDOS. A clear impression can be simply obtained by comparing the transmission and PDOS at a specific energy, for example, −0.05 eV, which corresponds to an energy point at the top of the valence band of spin up channel of the leads. In the meantime, −0.05 eV is also located in the original band gap of the pristine ZGNR which has an energy gap of 0.63 eV. The contribution of each edge C atom of the whole ZGNR to the PDOS of the central region at this energy is extracted and shown in figures 3(d)–(f). Obviously, for a pristine ZGNR, the PDOS of each edge C atom should be zero. However, it is not zero in the central region of our device and the decreasing trend as a function of the channel length nicely follows that of the transmission.

Consequently, in the following, we analyze the origin of finite PDOS of spin up in the central region in the original gap (0.63 eV) of the pristine ZGNR, which is key to understand the central results of all the above cases. There are two

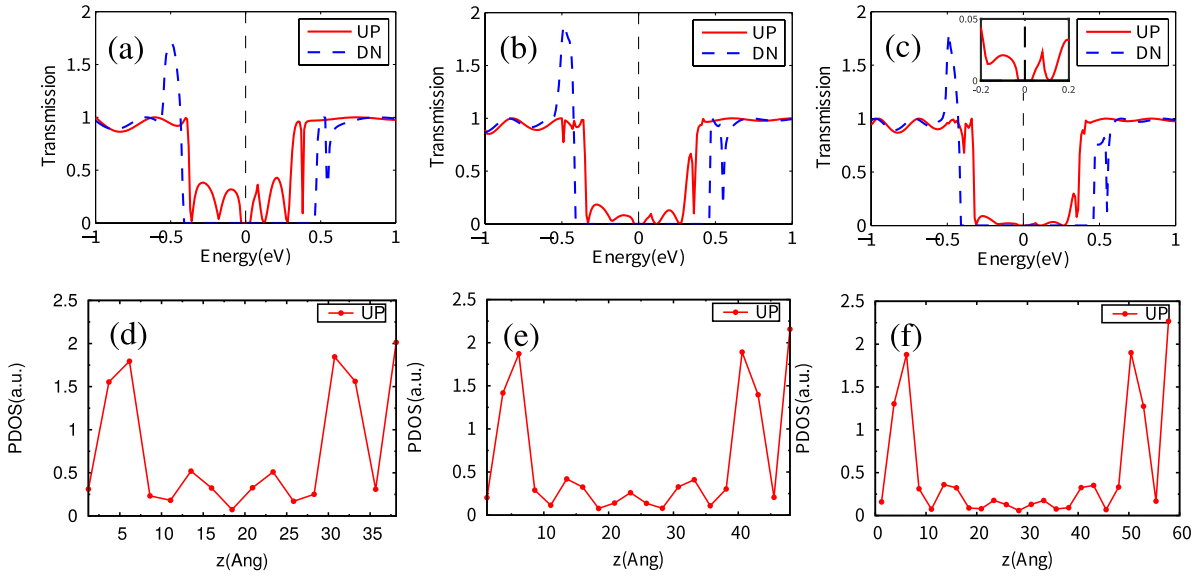

Figure 3. (a)–(c) The calculated equilibrium transmission functions for the transport junctions of different channel lengths with 8, 12 and 16 unit cells, respectively. (d)–(f) The calculated projected density of states at $E = -0.05$ eV for the transport junctions of different channel lengths with 8, 12 and 16 unit cells, respectively.

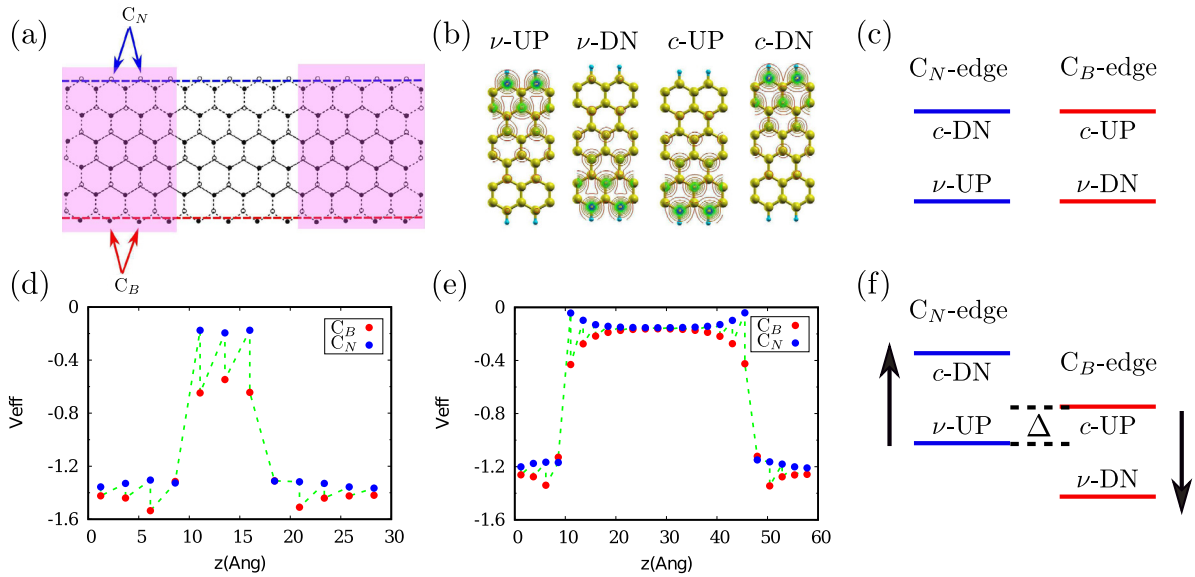

Figure 4. (a) Distribution of the edges states of the valence bands and conduction bands for the 6-ZGNR. 'ν' and 'c' indicate the valence band and conduction band, while 'UP' and 'DN' indicate the spin up and spin down channels, respectively. (b) The two sublattices labelled by C_B and C_N and the edge atomic sites indicated by two lines for which local potential will be extracted. (d), (e) The local potentials at the edge C_B and C_N atoms produced by the two BN layers, with channel length $n = 4$ and 16, respectively. (c), (f) A cartoon picture of the positions of the edge state valence band and conduction band before and after the interaction from the BN layers is considered. The two arrows indicate the shift direction of the energy of the edge states.

sublattices in both graphene and BN sheets. The two sublattices in the graphene can be labelled by C_B and C_N (see figure 4(a)), where the subscript 'B' or 'N' means each carbon atom in the sublattice is right located between two B or N atoms of the top and bottom BN layers. The top edge carbon atoms are C_N while the bottom edge carbon atoms are C_B. The appearance of PDOS in the original gap should be related to the energy shift of the edge states, but we need to reveal the mechanism. The spin up edge states of the valence band and the spin down edge states of the conduction band are localized at the top edge (see figures 4(b)(ν-UP) and (b)(c-DN)), while the spin down edge states of the valence band and the spin up edge states of the conduction band are localized at the bottom edge (see figures 4(b)(ν-DN) and (b)(c-UP)). The energy alignment of these edge states are schematically drawn by a cartoon in figure 4(c). These edge states will be affected by the potential produced by the BN sheets.

To have a full impression of the effects of BN sheets, we calculate the local potential distribution produced by the BN sheets on the two edge rows of carbon atoms in the whole central region, namely, the top edge C_N atoms and the bottom edge C_B atoms (see figure 4(b)). The local

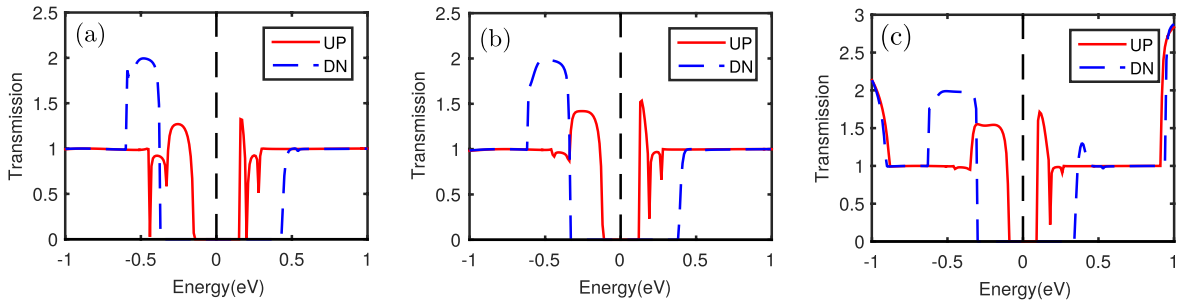

Figure 5. The transmission function with different channel width: (a) $n = 6$; (b) $n = 8$; (c) $n = 10$.

potential produced by the BN sheets at each atomic site is obtained by artificially taking away the graphene layer with the BN layers fixed and calculating the potential of the two BN layers, followed by averaging the potential around each site in a certain radius, which are shown in figures 4(d) and (e) for the channel length containing $n = 4$ and 16 unit cells of ZGNR. Clearly, for the $n = 4$ case, the local potential at the edge C_B sites is smaller than those at the edge C_N sites (see figure 4(d)), thus the edge states at the C_N are shifted up and the those at the C_B are shifted down in energy (see figure 4(e)), which results in the edge states of both the valence band and conduction band in the spin up channel shifting towards the Fermi level and the decrease of band gap Δ. The spin down edge states move away from the Fermi level and the corresponding band gap is increased, compared with original band gap of 0.63 eV. Consequently, due to the appearance of edge states in the gap, electrons can be transmitted from one lead to the other. However, with the increase of the channel length n, the potential difference between the C_N and C_B sublattices produced by the BN sheets decays exponentially towards the center of the channel region (see figure 4(f)), resulting in the length increase of the channel region in which the effects of the BN potential is negligible. It gives rise to the decrease of the PDOS at the center of the central region (see figures 3(d)–(f)) and the subsequent decrease of the transmission with the increase of the channel length (see figures 3(a)–(c)). With further increase of the channel length, the transmission gap of 0.63 eV will be recovered eventually.

Until now, our previous discussions are limited to the ribbon width $n = 6$. The effect of increasing ribbon width is also important for practical purposes. This effect can actually be reflected by studying the equilibrium transmission function. We will see the trend by increasing the ribbon width with number of zigzag chains w varying from 6 to 10. Thus, the transmission functions of the three cases for $w = 6, 8$ and 10, with the layer distance as 3.22 Å and the channel length $n = 4$, are shown in figure 5. It is seen that the $w = 8$ and 10 cases show very similar behaviors as the $w = 6$ case, which means that fully spin polarized transport can always be achieved at low bias with varying ribbon width. The main difference lies in the transmission gap decrease from $\Delta = 0.28$ eV to 0.24 and 0.19 eV with the increase of $w = 6$ to 8 and 10, respectively, which means the corresponding change in the threshold bias in the *I*–*V* curve.

Finally, all the investigations above have been performed under the condition of perfect edges. However, edge roughness or disorder may appear in a real device. Thus, we briefly discuss the effects of edge disorder in a qualitative way in the following. The edge disorder may appear in either ZGNRs or the h-BN nanoribbon. Such edge disorder factors in ZGNRs may cause the occurrence of localized states and breaking of edge states. The localized states may lead to the backscattering of electrons resulting in suppression of transmission and the breaking of edge states may lead to the decrease of energy difference between the AFM state and FM state. Both effects are detrimental to the observation of half-metallic transport. The edge disorder in h-BN nanoribbon may change the stagger potential imposed on the ZGNRs, and the relative changes in energy gap of different spin channels will be changed correspondingly, which will lead to the change of the transmission gap and the threshold voltage.

4. Conclusion

In summary, we have proposed a scheme of constructing zigzag edged graphene nanoribbons (ZGNR) transport junctions with *h*-BN/Gr/ *h*-BN vdW vertical vdW heterostructure leads for generating fully spin polarized current. Due to the different potential on the two sublattices of the whole zigzag graphene nanoribbon (ZGNR) produced by the BN sheets, the energy of the edge states with different spins is shifted towards opposite directions in the whole junction. This results in a decreased gap of spin up channel and an increased gap of spin down channel in both the leads and the central region, which makes fully spin polarized transport possible at low bias. The compression applied perpendicular to the vdW heterostructure leads significantly change the transport behavior of the heterojuncion in term of transmission magnitude and transmission gap. Decreasing the interlayer distance by 10% by compression leads to the closure of the transmission gap and the decrease of threshold bias to nearly zero. In addition, increasing the channel length will suppress the transmission and eventually recover the transmission gap of 0.63 eV, namely the band gap of the pristine ZGNR. These results suggest the great importance of *h*-BN/Gr/ *h*-BN vdW vertical vdW heterostructure in the design of ZGNR-based transport junction for generating fully spin polarized transport and the idea of vdW heterostructure in the design of spintronic devices based on two-dimensional materials.

Besides avoidance of atomic precision control of the doping or adsorption sites in chemical doping or magnetic atom adsorption scheme for achieving fully spin polarized transport in ZGNRs, another important advantage of using vdW structure is that it will not introduce any damage/change to the ZGNRs, so that the energy difference between the AFM and FM states will be basically unchanged, which is beneficial for the observation of half-metallic transport. In contrast, the decrease or disappearance of AFM-FM energy difference in chemical modification schemes is unavoidable [33]. Moreover, vdW vertical heterostructure is an emerging area in the study of 2D materials. It is highly desired to achieve new functions with the design of vdW vertical heterostructures. Our work provides a new example in this direction.

Acknowledgment

We gratefully acknowledge financial support by the National Natural Science Foundation of China under Grant Nos. 11574318(XZ), 11704232(LZ), 11374301(HH), 21503061(LS) and 11647147(JL); the Major/Innovative Program of Development Foundation of Hefei Center for Physical Science and Technology (under Grant No. 2016FXCX003) (XZ); Shanxi Science and Technology Department (No. 201701D121003)(LZ) and the Program of State Key Laboratory of Quantum Optics and Quantum Optics Devices (No: KF201810)(XZ and LZ); National Key R&D Program of China under Grants No. 2017YFA0304203(LZ) and No. 2016YFA0301700(LZ); Shanxi Province 100-Plan Talent Program(LZ). Calculations were performed in Center for Computational Science of CASHIPS, the ScGrid of Supercomputing Center and Computer Network Information Center of Chinese Academy of Sciences.

ORCID iDs

Peng Jiang https://orcid.org/0000-0002-4291-608X
Xiaohong Zheng https://orcid.org/0000-0002-3027-1042
Lei Zhang https://orcid.org/0000-0002-8634-8037

References

[1] de Groot R A, Mueller F M, Engen P G V and Buschow K H J 1983 *Phys. Rev. Lett.* **50** 2024
[2] Mallajosyula S S and Pati S K 2007 *J. Phys. Chem.* B **111** 13877
[3] Park J H, Vescovo E, Kim H J, Kwon C, Ramesh R and Venkatesan T 1998 *Nature* **392** 794
[4] Maslyuk V V, Bagrets A, Meded V, Arnold A, Evers F, Brandbyge M, Bredow T and Mertig I 2006 *Phys. Rev. Lett.* **97** 097201
[5] Son Y W, Cohen M L and Louie S G 2006 *Nature* **444** 347
[6] Kan E J, Wu X, Li Z, Zeng X C, Yang J and Hou J G 2008 *J. Chem. Phys.* **129** 084712
[7] Kan E J, Li Z, Yang J and Hou J G 2008 *J. Am. Chem. Soc.* **130** 4224
[8] Dutta S, Manna A K and Pati S K 2009 *Phys. Rev. Lett.* **102** 096601
[9] Zheng X H, Wang X L, Abtew T A and Zeng Z 2010 *J. Phys. Chem.* C **114** 4190
[10] Son Y W, Ihm J, Cohen M L, Louie S G and Choi H J 2005 *Phys. Rev. Lett.* **95** 216602
[11] Ponomarenko L *et al* 2011 *Nat. Phys.* **7** 958
[12] Britnell L *et al* 2012 *Science* **335** 947
[13] Dean C R *et al* 2010 *Nat. Nanotechnol.* **5** 722
[14] Haigh S, Gholinia A, Jalil R, Romani S, Britnell L, Elias D, Novoselov K, Ponomarenko L, Geim A and Gorbachev R 2012 *Nat. Mater.* **11** 764
[15] Li Q, Liu M, Zhang Y and Liu Z 2016 *Small* **12** 32
[16] Georgiou T *et al* 2013 *Nat. Nanotech.* **8** 100
[17] Geim A K and Grigorieva I V 2013 *Nature* **499** 419
[18] Liu Y, Weiss N O, Duan X, Cheng H C, Huang Y and Duan X 2016 *Nat. Rev. Mater.* **1** 16042
[19] Ghorbani-Asl M, Bristowe P D, Koziol K, Heine T and Kuc A 2016 *2D Mater.* **3** 025018
[20] Stradi D, Papior N R, Hansen O and Brandbyge M 2017 *Nano Lett.* **17** 2660
[21] Wang Y *et al* 2015 *Adv. Funct. Mater.* **25** 68
[22] Quhe R *et al* 2012 *NPG Asia Mater.* **4** e6
[23] Tao X, Zhang L, Zheng X, Hao H, Wang X, Song L, Zeng Z and Guo H 2018 *Nanoscale* **10** 174
[24] Ilyasov V V, Meshi B C, Nguyen V C, Ershov I V and Nguyen D C 2014 *J. Chem. Phys.* **141** 014708
[25] Barone V and Peralta J E 2008 *Nano Lett.* **8** 2210
[26] Zheng F, Zhou G, Liu Z, Wu J, Duan W, Gu B L and Zhang S B 2008 *Phys. Rev.* B **78** 205415
[27] Song L L, Zheng X H, Wang R L and Zeng Z 2010 *J. Phys. Chem.* C **114** 12145
[28] Yu J and Guo W 2013 *J. Phys. Chem. Lett.* **4** 951
[29] Maassen J, Harb M, Michaud-Rioux V, Zhu Y and Guo H 2013 *Proc. IEEE* **101** 518
[30] Taylor J, Guo H and Wang J 2001 *Phys. Rev.* B **63** 245407
[31] Soler J M, Artacho E, Gale J D, Garca A, Junquera J, Ordejn P and Snchez-Portal D 2002 *J. Phys.: Condens. Matter* **14** 2745
[32] Perdew J P, Burke K and Ernzerhof M 1996 *Phy. Rev. Lett.* **77** 3865
[33] Zheng X H, Wang X L, Huang L F, Hao H, Lan J and Zeng Z 2012 *Phys. Rev.* B **86** 081408